

# Spin-phonon coupling and thermal Hall effect in Kitaev spin liquid

Taekoo Oh<sup>\*,†</sup> and Naoto Nagaosa<sup>\*,†,‡</sup>

<sup>†</sup>*RIKEN Center for Emergent Matter Science (CEMS), Wako, Saitama 351-0198, Japan*

<sup>‡</sup>*Fundamental Quantum Science Program, TRIP Headquarters, RIKEN, Wako, Saitama,  
351-0198, Japan*

E-mail: taekoo.oh@riken.jp; nagaosa@riken.jp

## Abstract

Kitaev spin liquid (KSL), consisting of the bond direction-dependent spin interactions in the honeycomb lattice, attracts huge attention because of its exact solvability and prospect for applications to quantum computing. An important feature of KSL is the half-quantized thermal Hall conductivity (HQTHC) under the magnetic field perpendicular to the lattice, but HQTHC stands only at low temperatures. Here, in the temperature range beyond the HQTHC regime, we theoretically propose the extrinsic phonon contribution to thermal Hall Effect in KSL via the skew-scattering of chiral phonons by the scalar spin chirality, which was previously studied in Mott insulators. We show the emergence of the scalar spin chirality of fluctuating spins, estimate the emergent field strength and its symmetric form applied to the chiral phonons, and obtain the associated thermal Hall conductivity, which is semi-quantitatively consistent with the existing experiments. This work provides a basic understanding of the role of spin-phonon interactions in strongly correlated systems.

# Keywords

Kitaev spin liquid, thermal Hall Effect, chiral phonon, skew-scattering.

# Introduction

Kitaev spin liquid (KSL), composed of the spin exchange interactions depending on the bond direction on the honeycomb lattice<sup>1</sup> [See Fig. 1(a).], attracted huge attention in the last decades. The KSL under a magnetic field is modeled as<sup>2</sup>

$$H_0 = \sum_{\langle ij \rangle} J_{ij}^{\alpha_{ij}} \sigma_i^{\alpha_{ij}} \sigma_j^{\alpha_{ij}} - \frac{\vec{B}}{2} \cdot \sum_i \vec{\sigma}_i. \quad (1)$$

Here,  $\sigma_i^{\alpha_{ij}}$  is the spin-1/2 operators with  $\alpha_{ij} = x, y, z$ ,  $J_{ij}^{\alpha_{ij}} = J^x, J^y, J^z$  is the interaction strength, and  $\vec{B}$  is the magnetic field. Without the magnetic field, the Hamiltonian is exactly solvable by fractionalizing the spins into the Majorana fermions.<sup>1,3,4</sup> As shown in Fig. 1(b), when the interaction strength satisfies  $|J_x| \leq |J_y| + |J_z|$ ,  $|J_y| \leq |J_z| + |J_x|$ , and  $|J_z| \leq |J_x| + |J_y|$ , the spectrum of Majorana fermions becomes gapless ( $B$  phase), and vice versa ( $A_x, A_y, A_z$  phases). When the magnetic field  $\vec{B} \parallel [111]$  is applied to the gapless  $B$  phase, it opens a gap, and the unique excitations and their non-Abelian statistics take place.<sup>1,5</sup> This can be characterized by the emergence of edge modes and associated half-quantized thermal Hall Effect (HQTHE),<sup>1,6,7</sup> and also hint the application of KSL for quantum computing. Therefore, KSL has extensively been considered in both theories<sup>8-19</sup> and experiments.<sup>20-37</sup>

Especially in experiments, among the promising candidates,<sup>38</sup>  $\alpha$ -RuCl<sub>3</sub> was extensively investigated in the viewpoint of the thermal transport. In result, it was reported that the HQTHE was observed<sup>21,34</sup> in  $T \leq 6$  K with  $B \sim 8$  T. Moreover, as the thermal transport was also investigated up to  $T \sim 80$  K,<sup>23-25,32</sup> the features like  $\kappa_{yx}/T \sim 10^{-4}$  W/K<sup>2</sup>m, a peak near  $T = 20 \sim 30$  K, and a long tail up to  $T \approx 60 \sim 80$  K were observed. However, many intriguing issues still remain: the sample dependence of HQTHE,<sup>26,28,33,35</sup> the non-quantized thermal Hall conductivity

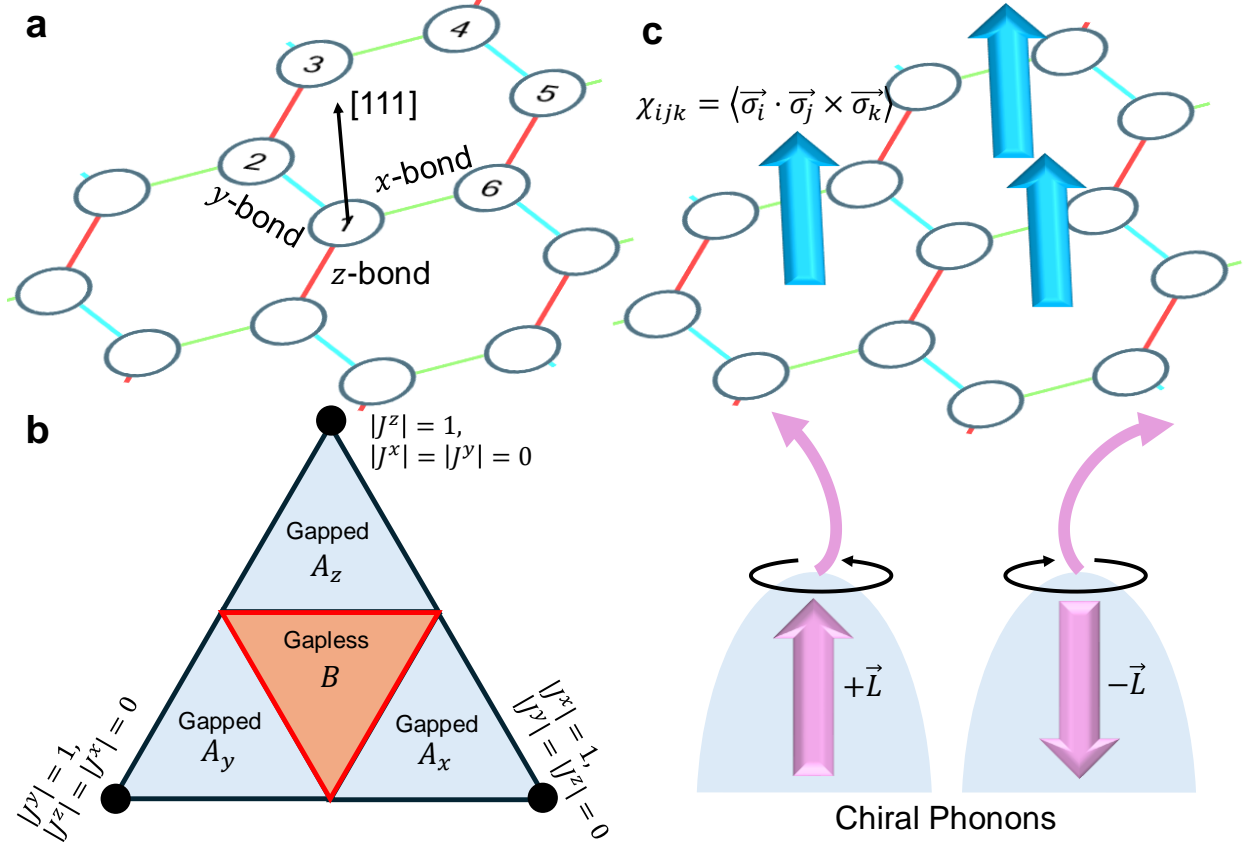


Figure 1: **Phonon thermal Hall Effect in Kitaev spin liquid.** (a) The schematics of Kitaev model. Green line is the  $x$ -bond, cyan line is the  $y$ -bond, and the red line is the  $z$ -bond. (b) The phase diagram of Kitaev model. The orange lines are the phase boundary  $|J^x| \leq |J^y| + |J^z|$ ,  $|J^y| \leq |J^z| + |J^x|$ , and  $|J^z| \leq |J^x| + |J^y|$ . Here, we concentrate on the gapless  $B$  phase in a magnetic field. (c) The schematics of the skew-scattering of chiral phonons by the scalar spin chirality.

(THC) by topological magnons,<sup>14</sup> and the large THC from Kitaev-Heisenberg paramagnons<sup>24,25</sup> and phonons.<sup>32</sup> Thus, there are still rooms for further investigations.

In this background, we propose the extrinsic origin of phonon thermal Hall Effect in the KSL with  $T > 10$  K, which is beyond the HQTHe regime. The mechanism is called the skew-scattering of chiral phonons by the scalar spin chirality (SSC) as shown in Fig. 1(c), which was previously known in multiferroic Mott insulators like  $\text{YMnO}_3$ .<sup>39,40</sup> The SSC  $\chi_{ijk} = \langle \vec{\sigma}_i \cdot \vec{\sigma}_j \times \vec{\sigma}_k \rangle$  is a composite order parameter defined by three different spins at  $i$ ,  $j$ , and  $k$  sites, which distinguishes the noncoplanar spin structure.<sup>41-48</sup> As it breaks the time-reversal symmetry, SSC can give rise to the transport phenomena like anomalous Hall and Nernst Effects.<sup>49-54</sup> In each plaquette of the lattice

under a magnetic field, the spin fluctuation can give rise to finite SSC. Because the electronic many-body wavefunction in each plaquette can be deformed by the finite SSC and the Berry connection emerges from the deformation, the emergent field that couples directly to the chiral phonon arises. Such a spin-phonon coupling, called Raman-type interaction,<sup>55,56</sup> scatter the chiral phonon with opposite angular momentum differently, inducing the sizable thermal Hall Effect from phonons as much as that from spins and magnons.<sup>57,58</sup> For an ideal case, the emergent field can rise up to 200 T and  $|\kappa_{yx}|$  can rise up to  $10^{-2}$  W/Km.<sup>40</sup>

Accordingly, we verify that the mechanism can also be effective in the KSL as follows. First, employing the exact diagonalization to Eq. (1), we compute the temperature and magnetic field dependence of the SSC in the KSL. Then, we estimate the emergent field strength and its symmetric form to settle down the Raman-type interaction. Lastly, the Raman-type interaction is employed in the semiclassical transport theory, and the THC is computed. We observe the features like  $\kappa_{yx}/T \sim 10^{-4}$  W/K<sup>2</sup>m, a peak near  $T = 15$  K, and a long tail up to 40 K, which are semi-quantitatively consistent with the experimental results in  $\alpha$ -RuCl<sub>3</sub>.

## Results

### The scalar spin chirality in Kitaev model

Primarily, let us study the temperature and magnetic field dependence of the SSC in the KSL model in Eq. (1). Previously, there are some theoretical reports that compute the SSC in the ground state of KSL models,<sup>10,18,19</sup> but here we focus on the finite temperature. We employ a total of 12 spins with  $2 \times 3$  unit cells of honeycomb lattice and compute the full spectrum  $\{E_i\}$  and corresponding eigenvectors  $\{|\psi_i\rangle\}$  by exact diagonalization. Also, we build the density matrix  $\rho = \sum_i \frac{e^{-\beta E_i}}{Z} |\psi_i\rangle \langle \psi_i|$  with  $Z = \sum_j e^{-\beta E_j}$ , and compute the SSC per plaquette  $\chi_p = \sum_{(abc)} \text{Tr}(\rho \vec{\sigma}_a \cdot \vec{\sigma}_b \times \vec{\sigma}_c)/6$  with the triangles  $(abc)$  shown in Fig. 2(a). We set  $J^x = J^y = J^z = J = \pm 5$  meV,  $10 \text{ K} < T < 60 \text{ K}$ , and  $0 \text{ T} < B < 17 \text{ T}$ , and  $\vec{B} \parallel [111]$ . Note that when  $\vec{B} \parallel [001]$  and its equivalent directions, the SSC vanishes.

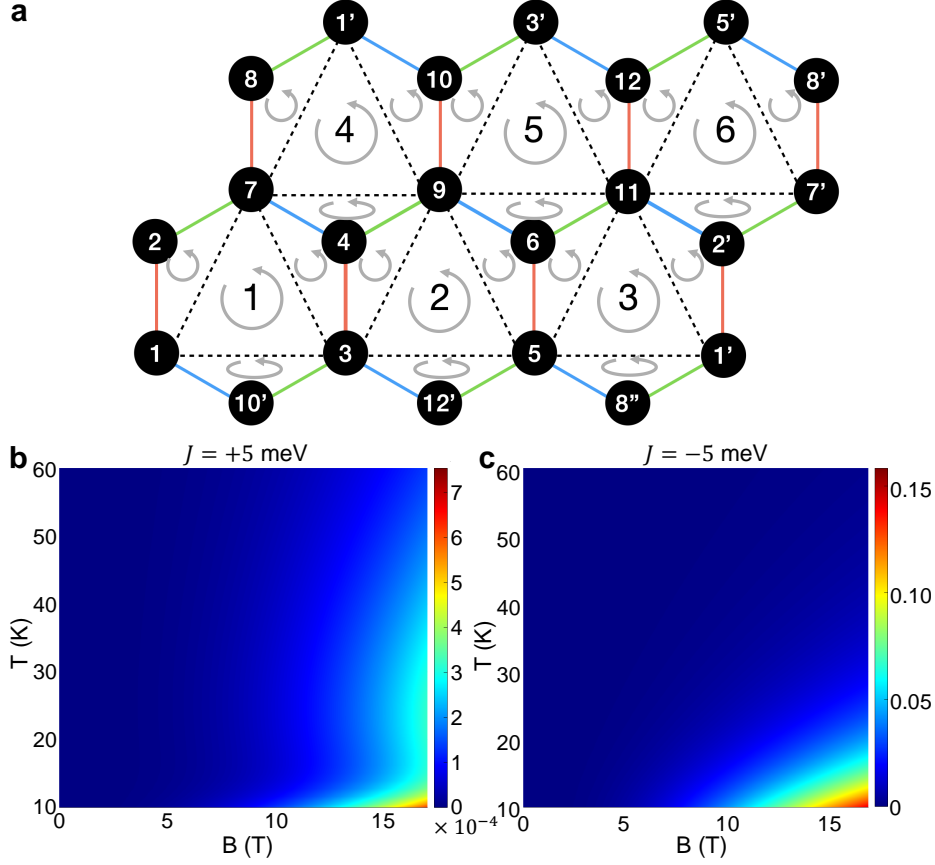


Figure 2: **The scalar spin chirality in Kitaev model.** (a) The schematics of  $2 \times 3$  unit cell (12 spins) in the periodic boundary condition. We divide each hexagon into four triangles and compute the SSC at each triangle. The direction of  $(abc)$  follows the gray arrows. We add up all SSC and acquire the SSC per hexagon  $\chi_p$ . (b-c) The SSC per hexagon  $\chi_p$  computed by the exact diagonalization as a function of magnetic field ( $B$ ) and temperature ( $T$ ), for (b)  $J = +5$  meV (antiferromagnetic) and (c)  $J = -5$  meV (ferromagnetic). Note that  $\alpha$ - $\text{RuCl}_3$  is modeled as ferromagnetic KSL.

The result is shown in Figs. 2(b-c). One can notice the following four aspects. First, the SSC is positive throughout all regions. Also, the SSC is one or two order larger in the ferromagnetic KSL,  $J = -5$  meV. Next, The SSC increases as magnetic field increases. Lastly, the SSC decreases as temperature increases. It is noteworthy that  $\alpha$ - $\text{RuCl}_3$  is modeled as the ferromagnetic KSL,<sup>59</sup> so one can expect that the SSC becomes effective in  $\alpha$ - $\text{RuCl}_3$  under a  $[111]$  magnetic field. Hence, we employ the results in the ferromagnetic KSL to investigate the emergent field and associated THC.

## The emergent field strength from the scalar spin chirality

As the SSC emerges in the KSL, the emergent field can arise from the SSC. Here, we estimate the emergent field strength and its symmetric form. Before proceeding, we briefly review the physics of emergent field and the Raman-type interaction.

The complete Hamiltonian for the solids is described by  $H = H_{\text{nu}} + H_{\text{el}} + V$ . Here,  $H_{\text{nu}} = -\sum_a \nabla_{\vec{R}_a}^2 / 2M_a$  is the nuclei kinetic energy,  $H_{\text{el}} = -\sum_i \nabla_{\vec{r}_i}^2 / 2m_e$  is the electron kinetic energy, and  $V = -\sum_{i,a} Z_a / r_{ia} + \sum_{i>j} 1 / r_{ij} + \sum_{a>b} Z_a Z_b / r_{ab}$  is the Coulomb interactions. Here,  $M_a$  is the nucleus mass,  $Z_a$  is the nucleus charge,  $m_e$  is the electron mass,  $\{\vec{r}_i\}$  is the electron positions, and  $\{\vec{R}_a\}$  is the nuclei positions. Since the electron energy is larger than that of phonons in the solids, one can apply the Born-Oppenheimer approximation,<sup>60</sup> in which the total wavefunction of  $H$  can be considered as a product of electronic and nuclei wavefunctions, i.e.,  $|\Psi\rangle \approx |\psi_{\text{el}}(\{\vec{r}_i\}, \{\vec{R}_a\})\rangle |\psi_{\text{nu}}(\{\vec{R}_a\})\rangle$ . One obtains the nuclei Hamiltonian by integrating out the electron wavefunction from  $H$ .

The Raman-type interaction can emerge when we include the correction term to the approximation. When the electron wavefunction is integrated out, one should keep the Berry connection from the wavefunction,  $\vec{a}_a = -i \langle \psi_{\text{el}} | \nabla_{\vec{R}_a} | \psi_{\text{el}} \rangle$ . This is because the ratio between the length scales of electron  $l_{\text{el}}$  and nuclei  $l_{\text{nu}}$  are not extremely different, such that  $l_{\text{el}} / l_{\text{nu}} = (M_a / m_e)^{1/4}$ . Accordingly, the corrected Born-Oppenheimer approximation becomes the following:<sup>56,61–64</sup>

$$H_{BO} = \sum_a \frac{(\vec{P}_a - Z_a \vec{A}_a - \vec{a}_a)^2}{2M_a} + E_{\text{el}}(\{\vec{R}_a\}). \quad (2)$$

Here,  $\vec{A}_a$  is the external vector potential,  $E_{\text{el}}(\{\vec{R}_a\})$  is the electronic energy with a fixed  $\{\vec{R}_a\}$ . In the single atom, the Berry connection completely cancels the external vector potential, describing the screening effect of electrons surrounding the nucleus. In the lattice, on the other hand, the cancellation is incomplete, so the Raman-type interaction  $\vec{P}_a \cdot \vec{a}'_a$  with  $\vec{a}'_a = Z_a \vec{A}_a + \vec{a}_a$  remains. The Raman-type interaction applies the emergent field  $\vec{B}_e = \nabla \times \vec{a}'_a$  to the  $a$ -th nucleus.

Keeping this in mind, let us estimate the emergent field strength. Here, we assume that the

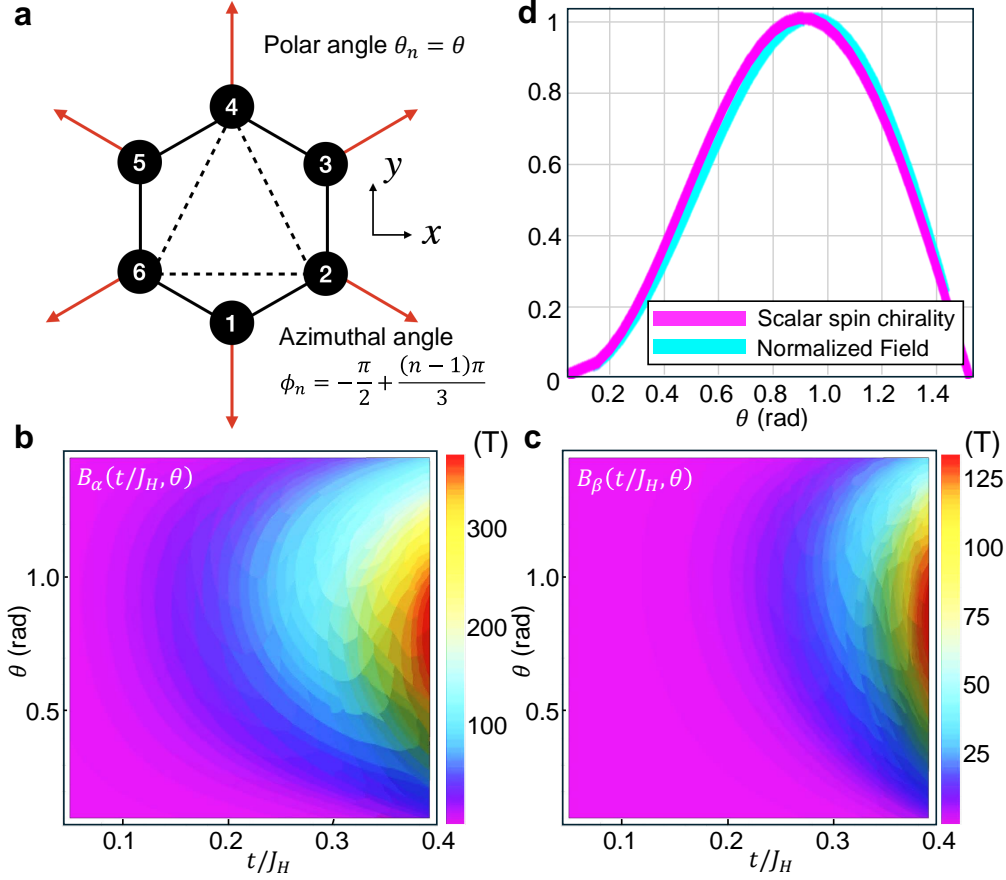


Figure 3: **The estimation of emergent field strength.** (a) The schematics of spin configuration in double exchange model. For  $n$ -th spin, the polar angle is  $\theta_n = \theta$  and the azimuthal angle is  $\phi_n = -\pi/2 + (n-1)\pi/3$ . (b-c) The emergent field strength from  $B_\alpha(t/J_H, \theta)$  and  $B_\beta(t/J_H, \theta)$  in Eq. (5) in the unit of tesla. (d) The comparison between  $\chi$  and normalized field strength at  $t/J_H = 0.23$  as a function of the polar angle  $\theta$ .

SSC from both quantum and classical spins can give rise to the emergent field and Raman-type interaction similarly. Hence, let us model the insulating state with the double exchange model with classical spins as follows.

$$H_1 = \sum_{ij} t_{ij} c_{i\alpha}^\dagger c_{j\alpha} - J_H \sum_i \vec{S}_i \cdot c_{i\alpha}^\dagger \vec{\sigma}_{i,\alpha\beta} c_{j\beta}. \quad (3)$$

Here,  $t_{ij}$  is the hopping integral between site  $i$  and  $j$ ,  $J_H$  is the double exchange strength,  $c_{i\alpha}$  is the electron operators,  $\vec{S}_i$  is the classical spins,  $\vec{\sigma}_i$  is the electron spins.  $t_{ij} = t + \delta t_{ij}(\{\vec{R}_a\})$  is divided into two parts, where  $t$  is the hopping integral at the equilibrium position while  $\delta t_{ij} \equiv$

$\delta t_{ij}(\{\vec{R}_a\})$  is the variation of hopping integral due to the nuclei displacement. We here assume that the hopping variation only depends on the nuclei position. The spin configuration is shown in Fig. 3(a), where the  $n$ -th spin in the hexagon has the polar angle  $\theta_n = \theta$  and the azimuthal angle  $\phi_n = -\pi/2 + (n-1)\pi/3$ . In this case, the total SSC of the hexagon is  $\chi = 3\sqrt{3} \cos \theta \sin^2 \theta$ . Since it is an insulator, the number of electrons is assumed to be six, which half-fills the system. Here, the control parameters are  $t/J_H \in (0, 0.4]$  and  $\theta \in (0, \pi/2)$ . We let  $J_H \approx 0.35$  eV according to the previous reports which is estimated from the Mott gap about  $U \approx 1.9$  eV.<sup>65-69</sup>

First, we acquire the second-order perturbed single-body eigenfunction  $|\varphi_\gamma\rangle \equiv |\varphi_\gamma(t/J_H, \delta t_{ij})\rangle$  ( $\gamma = 1, \dots, 12$ ) of  $H_1$  by considering  $\delta t_{ij}$  as perturbations. Then, the many-body wavefunction  $|\psi_{el}\rangle = \frac{1}{6!} \epsilon_{\gamma_1 \gamma_2 \gamma_3 \gamma_4 \gamma_5 \gamma_6} |\varphi_{\gamma_1}\rangle |\varphi_{\gamma_2}\rangle |\varphi_{\gamma_3}\rangle |\varphi_{\gamma_4}\rangle |\varphi_{\gamma_5}\rangle |\varphi_{\gamma_6}\rangle$  is given by the Slater determinant of eigenfunctions of six lowest single-body energies. Then, the Berry connection  $\vec{a}_a = -i \langle \psi_{el} | \nabla_{R_a} | \psi_{el} \rangle$  applied to  $a$ -th nucleus ( $a = 1, \dots, 6$ ) is given by

$$\vec{a}_a = \sum_{(ijklmn)} (\nabla_{R_a} \delta t_{ij}) [\alpha(t/J_H, \theta) (\delta t_{jk} - \delta t_{ni}) + \beta(t/J_H, \theta) (\delta t_{mn} - \delta t_{kl})], \quad (4)$$

with  $(ijklmn) = (123456)$  and its cyclic permutations. By approximating  $\delta t_{ij} \approx \nabla_{R_b} t_{ij} \cdot \vec{u}_b$  with the displacement  $\vec{u}_b$ , the emergent field strength  $B_e \approx B_\alpha + B_\beta$  can be estimated as

$$B_\alpha(t/J_H, \theta) \approx (\nabla_{R_a} \delta t_{ij})^2 \alpha(t/J_H, \theta), B_\beta(t/J_H, \theta) \approx (\nabla_{R_a} \delta t_{ij})^2 \beta(t/J_H, \theta). \quad (5)$$

By letting  $|\nabla_{R_a} \delta t_{ij}| \approx 100$  meV/Å,<sup>70</sup> we numerically acquire  $B_\alpha$  and  $B_\beta$  in Figs. 3(b-c) in the unit of tesla as a function of  $t/J_H$  and  $\theta$ . This increases as  $t/J_H$  increases and have a peak near  $\theta \approx 1$  when  $t/J_H \leq 0.3$ . It is worthy to note that the emergent field strength can increase up to few hundred teslas. Also, we compare the field strength at  $t/J_H = 0.23$  with the SSC in Fig. 3(d). Both show a peak near  $\theta \approx 1$  and vanishes at  $\theta = 0$  and  $\theta = \pi/2$ . This shows that the SSC and emergent field are correlated with each other.<sup>40</sup>



## The symmetric form of emergent field from the scalar spin chirality

However, the emergent field may vanish due to the symmetry. Eq. (4) vanishes when  $\delta t_{jk} = \delta t_{ni}$  and  $\delta t_{mn} = \delta t_{kl}$ . Therefore, when the nuclei displacement keeps the threefold rotation symmetry  $3_z$  about the  $z$ -axis,  $\vec{a}_a$  vanishes for all  $a$ . This fact necessitates the symmetry analysis to find the symmetric form of emergent field.

A honeycomb lattice has two sublattices  $A$  and  $B$  as shown in Fig. 4(a). It has space group  $P6/nmm$  and the point group of unit cell center is  $mmm$ .  $mmm$  group includes identity 1, twofold rotations  $2_x, 2_y, 2_z$ , inversion  $-1$ , and the mirrors  $m_x, m_y, m_z$ . Accordingly, the irreducible representations (IRREPs) are a total of 8, including  $A_g, B_{1g}, B_{2g}, B_{3g}, A_u, B_{1u}, B_{2u},$  and  $B_{3u}$ .<sup>71-73</sup> We classify the nuclei displacement and momentum in the  $xy$ -plane into the bases of IRREPs and showcase the classification in Fig. 4(a). For an IRREP  $\mathcal{R}$ , we denote the nuclei displacement  $U_{\mathcal{R}}$  and momentum  $P_{\mathcal{R}}$ . Explicitly, the classified nuclei displacements are represented as

$$U_{B_{3u}} = U_{A,x} + U_{B,x}, U_{B_{2u}} = U_{A,y} + U_{B,y}, U_{B_{1g}} = -U_{A,x} + U_{B,x}, U_{A_g} = -U_{A,y} + U_{B,y}. \quad (6)$$

Here,  $\vec{U}_A = (U_{A,x}, U_{A,y})$  and  $\vec{U}_B = (U_{B,x}, U_{B,y})$  are the displacement of each sublattice. The nuclei momentum has the same form as above except changing  $U$  to  $P$ . Also, we find that the SSC  $\chi$  in a hexagon corresponds to  $B_{1g}$ . Note that in the absence of spin-orbit coupling, any spin configuration except the SSC cannot couple to the phonons because phonons and SSC are invariant but the spin configurations are variant under any  $SO(3)$  global spin rotation.<sup>40,74-77</sup>

Then, there are two possible chiral phonons that can couple to the SSC,  $L_1 = U_{B_{3u}}P_{B_{2u}} - U_{B_{2u}}P_{B_{3u}}$  and  $L_2 = U_{B_{1g}}P_{A_g} - U_{A_g}P_{B_{1g}}$ . The chiral phonons  $L_1$  and  $L_2$  are shown in Figs. 4(b-c), respectively. However,  $L_1$  keeps the threefold rotation symmetry  $3_z$ , so the emergent field vanishes. Therefore, only  $L_2$  can couple to the emergent field by breaking  $3_z$ . Using Eq. (6), we can acquire the form of the Berry connection as

$$\vec{a}_A = \gamma\chi\hat{z} \times (\vec{U}_A - \vec{U}_B), \vec{a}_B = \gamma\chi\hat{z} \times (\vec{U}_B - \vec{U}_A). \quad (7)$$

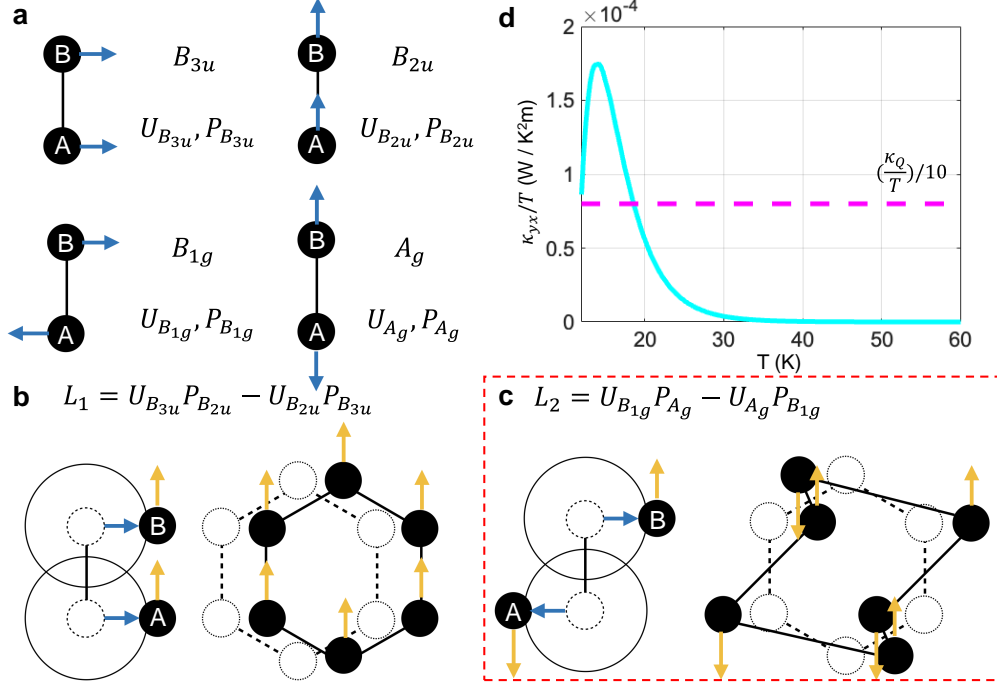


Figure 4: **The chiral phonon coupling to SSC and associated THC.** (a) The IRREP classification of nuclei displacement and momentum in the  $xy$ -plane. Here, the arrows represent either displacement and momentum. For IRREP  $\mathcal{R}$ , we denote the displacement  $U_{\mathcal{R}}$  and momentum  $P_{\mathcal{R}}$ , which is defined in Eq. (6). The SSC  $\chi$  is in  $B_{1g}$ . (b-c) The types of chiral phonons that can couple to the SSC. Here, blue arrows are the displacement, and yellow arrows are the momentum. However, for (b), since the threefold rotation symmetry is kept, the emergent field vanishes. Therefore, (c) with broken threefold rotation symmetry can couple to the SSC. (d) The computed THC from the acoustic phonon of honeycomb lattice (solid line) and its comparison with half-quantized THC  $\kappa_Q/T$  (dotted line). This shows the features like the peak near 20 K and the slow decay, which was observed in the experiments.

Here,  $\gamma$  is a constant. Thus, the emergent field is  $\vec{B}_e \propto \chi \hat{z}$ , and the form of Raman-type interaction is  $\vec{P}_A \cdot \vec{a}_A + \vec{P}_B \cdot \vec{a}_B$ .

## Estimation of the thermal Hall conductivity

Based on the form of emergent field, we can now acquire the THC from the phonon of honeycomb lattice. Primarily, we explain the honeycomb lattice phonon briefly. Previously, the phonon or sound velocity of  $\alpha$ -RuCl<sub>3</sub> are estimated as 4.4 km/s in longitudinal and 2.3 km/s in transverse directions.<sup>78,79</sup> We utilize the value and set the longitudinal spring constant  $K_{\parallel} = 167.78 \text{ meV/\AA}^2$  and transverse spring constant  $K_{\perp} = 22.37 \text{ meV/\AA}^2$ . Also, we adopt only two acoustic phonons

to compute the THC.

We employ the semiclassical Boltzmann scheme to acquire the THC. We denote  $\epsilon_l$  the phonon energy at band  $n$  and momentum  $\vec{k}$  with  $l = (n, k)$ ,  $f_l^0$  the Bose-Einstein distribution of phonon with energy  $\epsilon_l$ , and  $f_l = f_l^0 + g_l$  the nonequilibrium distribution with the deviation  $g_l$ . Then, the Boltzmann equation is reduced to the following with the relaxation time approximation.

$$\frac{\partial \epsilon_l}{\partial \vec{k}} \cdot \nabla_{\vec{r}} T \frac{\partial f_l^0}{\partial T} = -\frac{g_l}{\tau_0} - \sum_{l'} w_{ll'} g_{l'}. \quad (8)$$

Here,  $\tau_0 \sim 10^{-12}$  s is relaxation time of phonon, and  $w_{ll'}$  is the antisymmetric scattering matrix obtained by Fermi Golden rule and Born approximation. Explicitly,

$$\omega_{ll'} = 2\pi \sum_{l''} \left[ \left\{ \frac{\langle V_{l'l} V_{l''} V_{l''l'} \rangle}{\epsilon_{l'} - \epsilon_{l''} + i\eta} + c.c. \right\} - \left\{ \frac{\langle V_{l'l'} V_{l''} V_{l''l} \rangle}{\epsilon_l - \epsilon_{l''} + i\eta} + c.c. \right\} \right] \delta(\epsilon_l - \epsilon_{l'}). \quad (9)$$

Here,  $V_{ll'}$  is the impurity matrix by the emergent field. From Eq. (7) and the Raman-type interaction obtained above, the impurity matrix can be obtained as,

$$V_{ll'} = -B_e(T) \sum_{ab} \Gamma_{ab}(\mathcal{L}_{ab}^z)_{ll'} e^{i(\vec{k}' - \vec{k}) \cdot \vec{r}_a}, \quad (10)$$

where  $\Gamma_{ab} = \delta_{ab} - \sigma_{ab}^x$ , and  $\vec{\mathcal{L}}_{ab} = \vec{P}_a \times \vec{R}_b$  is the generalized phonon angular momentum. We consider the temperature-dependent emergent field  $B_e(T) = B_e(T = 10 \text{ K}) \chi(T) / \chi_{\max}$ , where  $\chi(T)$  comes from Fig. 2(c) at  $B = 15 \text{ T}$  and  $\chi_{\max}$  is the maximum value of  $\chi(T)$  in the temperature range. Comparing  $\chi_{\max} \approx 0.1$  at  $B = 15 \text{ T}$  and  $T = 10 \text{ K}$  in Fig. 2(c) with the field strength in Fig. 3, we assume that  $B_e(T = 10 \text{ K}) \approx 1.16 \text{ meV}$ . Then, the THC is computed as

$$\frac{\kappa_{yx}}{T} = -\frac{1}{T} \sum_l \epsilon_l \frac{\partial \epsilon_l}{\partial k_y} \frac{h_l}{\partial_x T}, \quad (11)$$

where  $h_l$  is the part of  $g_l$  that is the second order in relaxation time  $\tau_0$ .

The resulting  $\kappa_{yx}/T$  shown in Fig. 4(d). One can observe the following features. First, the

peak appears near  $T = 15$  K. Second, the decay is slow and the THC is finite below  $T = 40$  K. Third, the scale of  $\kappa_{yx}/T$  is close to  $10^{-4}$  W/K<sup>2</sup>m which is about one tenth of half-quantized THC  $\kappa_Q/T = \pi^2 k_B^2 / 6ha \approx 0.83$  mW/K<sup>2</sup>m with planck constant  $h$ , Boltzmann constant  $k_B$  and the lattice constant  $a$  of  $\alpha$ -RuCl<sub>3</sub>.<sup>30</sup> Intriguingly, these features semi-quantitatively agree with the experimental observations.<sup>23-25,32</sup> This fact implies that the mechanism for phonon thermal Hall Effect, the chiral phonon skew-scattering via the SSC, can be effective in the KSL.

## Discussion

In previous experiments,<sup>23-25,32</sup> the THC can appear up to  $T = 60 \sim 80$  K. Comparing to our results in Fig. 4(d) where the THC persists up to  $T = 40$  K, there can be the discrepancy. However, the discrepancy can be explained by the ruthenium ions. As the ruthenium atom is ionized in  $\alpha$ -RuCl<sub>3</sub>, the ions can directly couple to the magnetic field.<sup>55</sup> This can be a supplementary source of THC that fills the gap between experiments and our theory.

Also, as the chiral phonons with opposite angular momentums scatter differently by the SSC, the phonon angular momentum Hall Effect arises with the thermal Hall Effect.<sup>80</sup> Since phonon angular momentum can be piled up at the edges and couple to the circularly polarized light, the phonon angular momentum Hall Effect can be detected by shedding the circularly polarized light at opposite edges. The observation of phonon angular momentum Hall Effect under temperature gradient may evince that our mechanism happens in  $\alpha$ -RuCl<sub>3</sub>.

Most importantly, below  $T < 6$  K, we anticipate that the mechanism does not contribute much to the THC. If fixing the emergent field strength in temperatures, it is known that  $\kappa_{yx}/T \propto T^2$  at low temperatures.<sup>40</sup> Namely, as the phonon becomes inactive at the low temperatures,  $\kappa_{yx}/T$  converges to zero fast as temperature decreases. Therefore, this mechanism is compatible with the HQTHe below  $T < 6$  K.

So far, we suggest the extrinsic mechanism for phonon thermal Hall Effect in the temperature range beyond HQTHe, the skew-scattering of chiral phonons via the emergent field from the SSC.

We show the emergence of SSC in the KSL under [111] magnetic field, and find the strength and symmetric form of emergent field from the SSC. Using the symmetric form, we compute the THC semi-classically, and observe the features that are similar to the experimental results. By extending the work in a Mott insulator to the KSL, we provide further understanding of the spin-phonon interactions and its role in the thermal transport in strongly correlated systems.

## Acknowledgement

T.O. and N.N. were supported by JSPS KAKENHI Grant Numbers 24H00197 and 24H02231, and the RIKEN TRIP initiative.

## References

- (1) Kitaev, A. Anyons in an exactly solved model and beyond. *Annals of Physics* **2006**, *321*, 2–111.
- (2) Zhang, S.-S.; Halász, G. B.; Batista, C. D. Theory of the Kitaev model in a [111] magnetic field. *Nature Communications* **2022**, *13*, 399.
- (3) Feng, X.-Y.; Zhang, G.-M.; Xiang, T. Topological characterization of quantum phase transitions in a spin-1/2 model. *Physical review letters* **2007**, *98*, 087204.
- (4) Nasu, J.; Knolle, J.; Kovrizhin, D. L.; Motome, Y.; Moessner, R. Fermionic response from fractionalization in an insulating two-dimensional magnet. *Nature Physics* **2016**, *12*, 912–915.
- (5) Takagi, H.; Takayama, T.; Jackeli, G.; Khaliullin, G.; Nagler, S. E. Concept and realization of Kitaev quantum spin liquids. *Nature Reviews Physics* **2019**, *1*, 264–280.
- (6) Kane, C.; Fisher, M. P. Quantized thermal transport in the fractional quantum Hall effect. *Physical Review B* **1997**, *55*, 15832.

- (7) Cappelli, A.; Huerta, M.; Zemba, G. R. Thermal transport in chiral conformal theories and hierarchical quantum Hall states. *Nuclear Physics B* **2002**, *636*, 568–582.
- (8) Yao, H.; Kivelson, S. A. Exact chiral spin liquid with non-abelian anyons. *Physical review letters* **2007**, *99*, 247203.
- (9) Kim, H.-S.; Kee, H.-Y. Crystal structure and magnetism in  $\alpha$ -RuCl<sub>3</sub>: An ab initio study. *Physical Review B* **2016**, *93*, 155143.
- (10) Modic, K. A.; Ramshaw, B. J.; Shekhter, A.; Varma, C. M. Chiral spin order in some purported Kitaev spin-liquid compounds. *Physical Review B* **2018**, *98*, 205110.
- (11) Gordon, J. S.; Catuneanu, A.; Sørensen, E. S.; Kee, H.-Y. Theory of the field-revealed Kitaev spin liquid. *Nature communications* **2019**, *10*, 2470.
- (12) Gao, Y. H.; Hickey, C.; Xiang, T.; Trebst, S.; Chen, G. Thermal Hall signatures of non-Kitaev spin liquids in honeycomb Kitaev materials. *Physical Review Research* **2019**, *1*, 013014.
- (13) Takahashi, M. O.; Yamada, M. G.; Takikawa, D.; Mizushima, T.; Fujimoto, S. Topological nematic phase transition in Kitaev magnets under applied magnetic fields. *Physical Review Research* **2021**, *3*, 023189.
- (14) Zhang, E. Z.; Chern, L. E.; Kim, Y. B. Topological magnons for thermal Hall transport in frustrated magnets with bond-dependent interactions. *Physical Review B* **2021**, *103*, 174402.
- (15) Hwang, K.; Go, A.; Seong, J. H.; Shibauchi, T.; Moon, E.-G. Identification of a Kitaev quantum spin liquid by magnetic field angle dependence. *Nature communications* **2022**, *13*, 323.
- (16) Yılmaz, F.; Kampf, A. P.; Yip, S. K. Phase diagrams of Kitaev models for arbitrary magnetic field orientations. *Physical Review Research* **2022**, *4*, 043024.

- (17) Yu, S.-Y.; Li, H.; Zhao, Q.-R.; Gao, Y.; Dong, X.-Y.; Liu, Z.-X.; Li, W.; Gong, S.-S. Nematic chiral spin liquid in a Kitaev magnet under external magnetic field. *arXiv preprint arXiv:2304.00555* **2023**,
- (18) Luo, Q.; Zhao, J.; Li, J.; Wang, X. Chiral spin state and nematic ferromagnet in the spin-1 Kitaev- $\Gamma$  model. *Physical Review B* **2024**, *110*, 035121.
- (19) Holdhusen, W.; Huerga, D.; Ortiz, G. Emergent magnetic order in the antiferromagnetic Kitaev model in a [111] field. *Physical Review B* **2024**, *109*, 174411.
- (20) Banerjee, A.; Bridges, C.; Yan, J.-Q.; Aczel, A.; Li, L.; Stone, M.; Granroth, G.; Lumsden, M.; Yiu, Y.; Knolle, J., et al. Proximate Kitaev quantum spin liquid behaviour in a honeycomb magnet. *Nature materials* **2016**, *15*, 733–740.
- (21) Kasahara, Y.; Ohnishi, T.; Mizukami, Y.; Tanaka, O.; Ma, S.; Sugii, K.; Kurita, N.; Tanaka, H.; Nasu, J.; Motome, Y., et al. Majorana quantization and half-integer thermal quantum Hall effect in a Kitaev spin liquid. *Nature* **2018**, *559*, 227–231.
- (22) McClarty, P.; Dong, X.-Y.; Gohlke, M.; Rau, J.; Pollmann, F.; Moessner, R.; Penc, K. Topological magnons in Kitaev magnets at high fields. *Physical Review B* **2018**, *98*, 060404.
- (23) Kasahara, Y.; Sugii, K.; Ohnishi, T.; Shimozawa, M.; Yamashita, M.; Kurita, N.; Tanaka, H.; Nasu, J.; Motome, Y.; Shibauchi, T., et al. Unusual thermal Hall effect in a Kitaev spin liquid candidate  $\alpha$ -RuCl<sub>3</sub>. *Physical review letters* **2018**, *120*, 217205.
- (24) Hentrich, R.; Wolter, A. U.; Zotos, X.; Brenig, W.; Nowak, D.; Isaeva, A.; Doert, T.; Banerjee, A.; Lampen-Kelley, P.; Mandrus, D. G., et al. Unusual phonon heat transport in  $\alpha$ -RuCl<sub>3</sub>: strong spin-phonon scattering and field-induced spin gap. *Physical review letters* **2018**, *120*, 117204.
- (25) Hentrich, R.; Roslova, M.; Isaeva, A.; Doert, T.; Brenig, W.; Büchner, B.; Hess, C. Large ther-

- mal Hall effect in  $\alpha$ -RuCl<sub>3</sub>: Evidence for heat transport by Kitaev-Heisenberg paramagnons. *Physical Review B* **2019**, *99*, 085136.
- (26) Yamashita, M.; Gouchi, J.; Uwatoko, Y.; Kurita, N.; Tanaka, H. Sample dependence of half-integer quantized thermal Hall effect in the Kitaev spin-liquid candidate  $\alpha$ -RuCl<sub>3</sub>. *Physical Review B* **2020**, *102*, 220404.
- (27) Sears, J. A.; Chern, L. E.; Kim, S.; Bereciartua, P. J.; Francoual, S.; Kim, Y. B.; Kim, Y.-J. Ferromagnetic Kitaev interaction and the origin of large magnetic anisotropy in  $\alpha$ -RuCl<sub>3</sub>. *Nature physics* **2020**, *16*, 837–840.
- (28) Czajka, P.; Gao, T.; Hirschberger, M.; Lampen-Kelley, P.; Banerjee, A.; Yan, J.; Mandrus, D. G.; Nagler, S. E.; Ong, N. Oscillations of the thermal conductivity in the spin-liquid state of  $\alpha$ -RuCl<sub>3</sub>. *Nature Physics* **2021**, *17*, 915–919.
- (29) Wang, Y.; Jin, Y.; Wang, L.; Hao, Z.; Liu, C.; Hao, Y.-J.; Ma, X.-M.; Kumar, S.; Schwier, E. F.; Shimada, K., et al. Evidence of Weyl fermions in  $\alpha$ -RuCl<sub>3</sub>. *Physical Review B* **2021**, *103*, 035150.
- (30) Yokoi, T.; Ma, S.; Kasahara, Y.; Kasahara, S.; Shibauchi, T.; Kurita, N.; Tanaka, H.; Nasu, J.; Motome, Y.; Hickey, C., et al. Half-integer quantized anomalous thermal Hall effect in the Kitaev material candidate  $\alpha$ -RuCl<sub>3</sub>. *Science* **2021**, *373*, 568–572.
- (31) Suetsugu, S.; Ukai, Y.; Shimomura, M.; Kamimura, M.; Asaba, T.; Kasahara, Y.; Kurita, N.; Tanaka, H.; Shibauchi, T.; Nasu, J., et al. Evidence for a phase transition in the quantum spin liquid state of a Kitaev candidate  $\alpha$ -RuCl<sub>3</sub>. *Journal of the Physical Society of Japan* **2022**, *91*, 124703.
- (32) Lefrançois, É.; Grissonnanche, G.; Baglo, J.; Lampen-Kelley, P.; Yan, J.-Q.; Balz, C.; Mandrus, D.; Nagler, S.; Kim, S.; Kim, Y.-J., et al. Evidence of a phonon Hall effect in the Kitaev spin liquid candidate  $\alpha$ -RuCl<sub>3</sub>. *Physical Review X* **2022**, *12*, 021025.



- (33) Kasahara, Y.; Suetsugu, S.; Asaba, T.; Kasahara, S.; Shibauchi, T.; Kurita, N.; Tanaka, H.; Matsuda, Y. Quantized and unquantized thermal Hall conductance of the Kitaev spin liquid candidate  $\alpha$ -RuCl<sub>3</sub>. *Physical Review B* **2022**, *106*, L060410.
- (34) Bruin, J. A. N.; Claus, R. R.; Matsumoto, Y.; Kurita, N.; Tanaka, H.; H., T. Robustness of the thermal Hall effect close to half-quantization in  $\alpha$ -RuCl<sub>3</sub>. *Nature Physics* **2022**, *18*, 401–405.
- (35) Zhang, H.; May, A. F.; Miao, H.; Sales, B. C.; Mandrus, D. G.; Nagler, S. E.; McGuire, M. A.; Yan, J. Sample-dependent and sample-independent thermal transport properties of  $\alpha$ -RuCl<sub>3</sub>. *Physical Review Materials* **2023**, *7*, 114403.
- (36) Czajka, P.; Gao, T.; Hirschberger, M.; Lampen-Kelley, P.; Banerjee, A.; Quirk, N.; Mandrus, D. G.; Nagler, S. E.; Ong, N. P. Planar thermal Hall effect of topological bosons in the Kitaev magnet  $\alpha$ -RuCl<sub>3</sub>. *Nature Materials* **2023**, *22*, 36–41.
- (37) Imamura, K.; Suetsugu, S.; Mizukami, Y.; Yoshida, Y.; Hashimoto, K.; Ohtsuka, K.; Kasahara, Y.; Kurita, N.; Tanaka, H.; Noh, P., et al. Majorana-fermion origin of the planar thermal Hall effect in the Kitaev magnet  $\alpha$ -RuCl<sub>3</sub>. *Science advances* **2024**, *10*, eadk3539.
- (38) Trebst, S.; Hickey, C. Kitaev materials. *Physics Reports* **2022**, *950*, 1–37.
- (39) Kim, H.-L.; Saito, T.; Yang, H.; Ishizuka, H.; Coak, M. J.; Lee, J. H.; Sim, H.; Oh, Y. S.; Nagaosa, N.; Park, J.-G. Thermal Hall effects due to topological spin fluctuations in YMnO<sub>3</sub>. *Nature Communications* **2024**, *15*, 243.
- (40) Oh, T.; Nagaosa, N. Phonon thermal Hall effect in Mott insulators via skew-scattering by the scalar spin chirality. *arXiv preprint arXiv:2408.01671* **2024**,
- (41) Wen, X.-G.; Wilczek, F.; Zee, A. Chiral spin states and superconductivity. *Physical Review B* **1989**, *39*, 11413.
- (42) Kawamura, H. Chiral ordering in Heisenberg spin glasses in two and three dimensions. *Physical review letters* **1992**, *68*, 3785.

- (43) Shindou, R.; Nagaosa, N. Orbital ferromagnetism and anomalous Hall effect in antiferromagnets on the distorted fcc lattice. *Physical review letters* **2001**, *87*, 116801.
- (44) Taguchi, Y.; Oohara, Y.; Yoshizawa, H.; Nagaosa, N.; Tokura, Y. Spin chirality, Berry phase, and anomalous Hall effect in a frustrated ferromagnet. *Science* **2001**, *291*, 2573–2576.
- (45) Lee, P. A.; Nagaosa, N.; Wen, X.-G. Doping a Mott insulator: Physics of high-temperature superconductivity. *Reviews of modern physics* **2006**, *78*, 17–85.
- (46) Kawamura, H. Chirality scenario of the spin-glass ordering. *Journal of the Physical Society of Japan* **2010**, *79*, 011007.
- (47) Nagaosa, N.; Yu, X.; Tokura, Y. Gauge fields in real and momentum spaces in magnets: monopoles and skyrmions. *Philosophical Transactions of the Royal Society A: Mathematical, Physical and Engineering Sciences* **2012**, *370*, 5806–5819.
- (48) Nagaosa, N.; Tokura, Y. Emergent electromagnetism in solids. *Physica Scripta* **2012**, *2012*, 014020.
- (49) Bruno, P.; Dugaev, V.; Taillefumier, M. Topological Hall effect and Berry phase in magnetic nanostructures. *Physical review letters* **2004**, *93*, 096806.
- (50) Neubauer, A.; Pfleiderer, C.; Binz, B.; Rosch, A.; Ritz, R.; Niklowitz, P.; Böni, P. Topological Hall effect in the A phase of MnSi. *Physical review letters* **2009**, *102*, 186602.
- (51) Nagaosa, N.; Sinova, J.; Onoda, S.; MacDonald, A. H.; Ong, N. P. Anomalous hall effect. *Reviews of modern physics* **2010**, *82*, 1539–1592.
- (52) Kanazawa, N.; Onose, Y.; Arima, T.; Okuyama, D.; Ohoyama, K.; Wakimoto, S.; Kakurai, K.; Ishiwata, S.; Tokura, Y. Large topological Hall effect in a short-period helimagnet MnGe. *Physical review letters* **2011**, *106*, 156603.
- (53) Ishizuka, H.; Nagaosa, N. Spin chirality induced skew scattering and anomalous Hall effect in chiral magnets. *Science advances* **2018**, *4*, eaap9962.

- (54) Ishizuka, H.; Nagaosa, N. Large anomalous Hall effect and spin Hall effect by spin-cluster scattering in the strong-coupling limit. *Physical Review B* **2021**, *103*, 235148.
- (55) Agarwalla, B. K.; Zhang, L.; Wang, J.-S.; Li, B. Phonon Hall effect in ionic crystals in the presence of static magnetic field. *The European Physical Journal B* **2011**, *81*, 197–202.
- (56) Saito, T.; Misaki, K.; Ishizuka, H.; Nagaosa, N. Berry phase of phonons and thermal Hall effect in nonmagnetic insulators. *Physical Review Letters* **2019**, *123*, 255901.
- (57) Katsura, H.; Nagaosa, N.; Lee, P. A. Theory of the thermal Hall effect in quantum magnets. *Physical review letters* **2010**, *104*, 066403.
- (58) Onose, Y.; Ideue, T.; Katsura, H.; Shiomi, Y.; Nagaosa, N.; Tokura, Y. Observation of the magnon Hall effect. *Science* **2010**, *329*, 297–299.
- (59) Kim, S.; Yuan, B.; Kim, Y.-J.  $\alpha$ -RuCl<sub>3</sub> and other Kitaev materials. *APL Materials* **2022**, *10*.
- (60) Oppenheimer, M. Zur Quantentheorie der Molekeln [On the quantum theory of molecules]. *Annalen der Physik* **1927**, *389*, 457–484.
- (61) Mead, C. A.; Truhlar, D. G. On the determination of Born–Oppenheimer nuclear motion wave functions including complications due to conical intersections and identical nuclei. *The Journal of Chemical Physics* **1979**, *70*, 2284–2296.
- (62) Mead, C. A. The geometric phase in molecular systems. *Reviews of modern physics* **1992**, *64*, 51.
- (63) Zhang, L.; Ren, J.; Wang, J.-S.; Li, B. Topological nature of the phonon Hall effect. *Physical review letters* **2010**, *105*, 225901.
- (64) Qin, T.; Zhou, J.; Shi, J. Berry curvature and the phonon Hall effect. *Physical Review B—Condensed Matter and Materials Physics* **2012**, *86*, 104305.
- (65) Rojas, S.; Spinolo, G. Hall effect in  $\alpha$ -RuCl<sub>3</sub>. *Solid state communications* **1983**, *48*, 349–351.

- (66) Plumb, K.; Clancy, J.; Sandilands, L.; Shankar, V. V.; Hu, Y.; Burch, K.; Kee, H.-Y.; Kim, Y.-J.  $\alpha$ -RuCl<sub>3</sub>: A spin-orbit assisted Mott insulator on a honeycomb lattice. *Physical Review B* **2014**, *90*, 041112.
- (67) Sandilands, L. J.; Tian, Y.; Reijnders, A. A.; Kim, H.-S.; Plumb, K. W.; Kim, Y.-J.; Kee, H.-Y.; Burch, K. S. Spin-orbit excitations and electronic structure of the putative Kitaev magnet  $\alpha$ -RuCl<sub>3</sub>. *Physical Review B* **2016**, *93*, 075144.
- (68) Zhou, X.; Li, H.; Waugh, J.; Parham, S.; Kim, H.-S.; Sears, J.; Gomes, A.; Kee, H.-Y.; Kim, Y.-J.; Dessau, D. Angle-resolved photoemission study of the Kitaev candidate  $\alpha$ -RuCl<sub>3</sub>. *Physical Review B* **2016**, *94*, 161106.
- (69) Sinn, S.; Kim, C. H.; Kim, B. H.; Lee, K. D.; Won, C. J.; Oh, J. S.; Han, M.; Chang, Y. J.; Hur, N.; Sato, H., et al. Electronic structure of the Kitaev material  $\alpha$ -RuCl<sub>3</sub> probed by photoemission and inverse photoemission spectroscopies. *Scientific reports* **2016**, *6*, 39544.
- (70) Coropceanu, V.; Cornil, J.; da Silva Filho, D. A.; Olivier, Y.; Silbey, R.; Brédas, J.-L. Charge transport in organic semiconductors. *Chemical reviews* **2007**, *107*, 926–952.
- (71) Aroyo, M. I.; Perez-Mato, J. M.; Capillas, C.; Kroumova, E.; Ivantchev, S.; Madariaga, G.; Kirov, A.; Wondratschek, H. Bilbao Crystallographic Server: I. Databases and crystallographic computing programs. *Zeitschrift für Kristallographie-Crystalline Materials* **2006**, *221*, 15–27.
- (72) Aroyo, M. I.; Kirov, A.; Capillas, C.; Perez-Mato, J.; Wondratschek, H. Bilbao Crystallographic Server. II. Representations of crystallographic point groups and space groups. *Acta Crystallographica Section A: Foundations of Crystallography* **2006**, *62*, 115–128.
- (73) Aroyo, M. I.; Perez-Mato, J. M.; Orobengoa, D.; Tasci, E.; de la Flor, G.; Kirov, A. Crystallography online: Bilbao crystallographic server. *Bulg. Chem. Commun* **2011**, *43*, 183–197.

- (74) Suzuki, M.-T.; Koretsune, T.; Ochi, M.; Arita, R. Cluster multipole theory for anomalous Hall effect in antiferromagnets. *Physical Review B* **2017**, *95*, 094406.
- (75) Oh, T.; Ishizuka, H.; Yang, B.-J. Magnetic field induced topological semimetals near the quantum critical point of pyrochlore iridates. *Physical Review B* **2018**, *98*, 144409.
- (76) Suzuki, M.-T.; Nomoto, T.; Arita, R.; Yanagi, Y.; Hayami, S.; Kusunose, H. Multipole expansion for magnetic structures: a generation scheme for a symmetry-adapted orthonormal basis set in the crystallographic point group. *Physical Review B* **2019**, *99*, 174407.
- (77) Oh, T.; Park, S.; Yang, B.-J. Transverse Magnetization in Spin-Orbit Coupled Antiferromagnets. *Physical Review Letters* **2023**, *130*, 266703.
- (78) Lebert, B. W.; Kim, S.; Prishchenko, D. A.; Tsirlin, A. A.; Said, A. H.; Alatas, A.; Kim, Y.-J. Acoustic phonon dispersion of  $\alpha$ -RuCl<sub>3</sub>. *Physical Review B* **2022**, *106*, L041102.
- (79) Mu, S.; Dixit, K. D.; Wang, X.; Abernathy, D. L.; Cao, H.; Nagler, S. E.; Yan, J.; Lampen-Kelley, P.; Mandrus, D.; Polanco, C. A., et al. Role of the third dimension in searching for Majorana fermions in  $\alpha$ -RuCl<sub>3</sub> via phonons. *Physical Review Research* **2022**, *4*, 013067.
- (80) Park, S.; Yang, B.-J. Phonon angular momentum Hall effect. *Nano Letters* **2020**, *20*, 7694–7699.

# TOC Graphic

